ELSEVIER

Journal of Molecular Catalysis A: Chemical 163 (2000) 91–103

JOURNAL OF MOLECULAR CATALYSIS A: CHEMICAL

www.elsevier.com/locate/molcata

Ethane hydrogenolysis over platinum Selection and estimation of kinetic parameters

R.D. Cortright, R.M. Watwe, J.A. Dumesic*

Department of Chemical Engineering, University of Wisconsin-Madison, Madison, WI 53706, USA

Received 2 February 2000; accepted 8 May 2000

Abstract

Kinetic models are formulated to describe the essential surface chemistry involved in ethane hydrogenolysis over platinum catalysts, through consolidation of results obtained from first principles calculations and reaction kinetics studies. Quantum chemical calculations based on density functional theory (DFT) were conducted to probe the structures and energetics of various adsorbed C_2H_x species on platinum, as well as activated complexes involved in cleavage of the C–C bond. De Donder relations were used to identify kinetic coefficients that minimize complications from unintentional compensation effects. Results from DFT calculations and kinetic analyses suggest that the most abundant surface species during ethane hydrogenolysis are adsorbed atomic hydrogen and highly dehydrogenated hydrocarbon species (e.g. ethylidyne species), whereas the primary reaction pathways for cleavage of the C–C bond on Pt take place through transition states that are more highly hydrogenated (e.g. C_2H_5 and $CHCH_3$ species). The results from DFT calculations indicate that C_2H_x adsorbed species and transition states interact more strongly with Pt(2 1 1) than with Pt(1 1 1) surfaces, in agreement with the known structure sensitivity of ethane hydrogenolysis over Pt catalysts.

Keywords: Kinetic analysis; DFT; Ethane hydrogenolysis; Platinum; De Donder

1. Introduction

Catalytic processes on surfaces take place through sequences of elementary reactions involving adsorbed reactants, products, and reaction intermediates associated with active sites on the catalyst surface. Studies of chemical kinetics of catalytic processes, thus, typically involve analyses of reaction schemes, with the aim of describing the rate of the overall reaction in terms of contributions from individual elementary steps. While in the most general case it is desirable to determine pre-exponential factors and activation energies for each of these elementary steps, there is usually not sufficient information to extract the values of all kinetic parameters. Accordingly, there is an information-deficit that requires a compromise between the desire to include chemical detail in the reaction scheme and the realization that the observed reaction kinetics is controlled by a limited number of kinetic parameters. In this respect, several issues become important. For example, what elementary steps are kinetically important, and how many kinetic parameters are required to capture the observed chemistry of a given catalytic process?

During the past several years, significant advances have been made in the applications of quantum chemical techniques to identify the geometries, energetics and vibrational modes of chemical species interacting with catalytic sites consisting of clusters

* Corresponding author. Tel.: +1-608-262-1095; fax: +1-608-262-5434.

1381-1169/00/$ – see front matter
PII: S1381-1169(00)00402-7

or periodic arrangements of atoms [1,2]. In addition, considerable information about the properties of chemical species on catalyst surfaces is available from experimental studies [3,4]. This increasing availability of energetic and entropic information obtained from theoretical and experimental studies is invaluable in kinetic analyses to minimize the information-deficit and to help determine which of the kinetic parameters are important in controlling catalyst performance.

An important consequence of conducting kinetic analyses in conjunction with results from quantum chemical calculations and experimental studies of surface species is that quantitative knowledge about the catalytic process is built at the molecular level into the kinetic model. In fact, one of the difficulties encountered when trying to utilize reaction kinetic data collected for a particular catalyst system to assist in the development of another catalyst system is that a common basis for comparison between the systems cannot be identified. For example, the active sites may have different structures; the reaction sequences may involve different reaction intermediates; the surface coverage regimes may be different. Without a means to account for the key differences between the catalyst systems, it is not possible to take advantage of the similarities that these systems may possess. However, by extracting information about the catalyst system at the molecular level, it may be possible to identify the common factors that control the nature and the strength of the chemical bonding in both catalyst systems. This process of extracting fundamental knowledge from experimental information, therefore, provides a molecular-level basis for comparison between catalyst systems, and it provides unifying principles for the design of new catalyst systems.

In the present paper, the combined results from experimental and theoretical investigations are consolidated with the aim of interpreting the observed reaction kinetics data for ethane hydrogenolysis over platinum. Ethane hydrogenolysis has been a bellwether probe reaction to investigate the reactivities of hydrocarbons over metal catalysts [5–14]. To this day, investigators have conducted analyses of kinetic data for ethane hydrogenolysis using models based on the following two-step reaction scheme proposed by Cimino et al. [15]:

$$C_2H_6 \rightleftharpoons C_2H_x(\text{ads}) + \left(\frac{6-x}{2}\right)H_2$$

$$C_2H_x(\text{ads}) + H_2 \rightarrow CH_4$$

where the first step is quasi-equilibrated and the second step is irreversible. This scheme leads to a rate expression of the power-law form:

$$\text{rate} = kP_E^n P_H^{1-na} \quad (1)$$

where a is equal to $(6-x)/2$ and P_E and P_H are the partial pressures of ethane and dihydrogen, respectively. Over the years, this two-step mechanism has been modified to incorporate such features such as competitive adsorption of hydrogen and cleavage of the C–C bond through interaction with either gaseous dihydrogen, surface atomic hydrogen, or vacant surface sites (as reviewed by Shang and Kenney [13]). However, two main features of the model have been maintained: (1) the most abundant reactive intermediate is formed in quasi-equilibrium with gas-phase ethane and dihydrogen, and (2) this same reactive intermediate is involved in the rate-limiting C–C bond cleavage step. In this paper, we show that the reactive intermediates are not necessarily the most abundant surface intermediates.

The present paper begins with a detailed reaction scheme to describe the results of a previously reported kinetic study of ethane hydrogenolysis over platinum [14], and uses recent results from quantum chemical calculations employing density functional theory (DFT) [16] to provide initial guesses for the kinetic parameters of this system. In addition, the present paper uses reaction schemes involving the quasi-equilibrated formation of reaction intermediates and transitions states from gaseous ethane and dihydrogen, as identified using the concepts of De Donder [17–21]. Moreover, the use of De Donder relations provides a simple means to determine the number of kinetic parameters required to calculate the overall reaction rate from a reaction scheme.

2. Kinetic analyses

2.1. De Donder analyses

According to the De Donder relation, we write the net rate for elementary step i in terms of the forward

rate of the step, $\vec{r}_i$, and the affinity for the step, A_i:

$$r_i = \vec{r}_i \left[1 - \exp\left(\frac{-A_i}{RT}\right)\right] \quad (2)$$

where the affinity is equal to minus the change in the Gibbs free energy with respect to the extent of reaction (i.e. equal to the difference in the Gibbs free energies of the reactants and products of the elementary step at the reaction temperature and at the corresponding partial pressure for each reactant, product, and reaction intermediate). In general, the affinity, A_i, is expressed in terms of the standard state Gibbs free energies, G_j^o, and the activities, a_j, of the j reactants and products of the step

$$A_i = -\sum_j \upsilon_{ij} G_j = -\sum_j \upsilon_{ij}[G_j^o + RT\ln(a_j)] \quad (3)$$

where υ_{ij} are the stoichiometric coefficients for the j reactants and products of step i. This expression can be written in terms of the equilibrium coefficient for the step, $K_{i\,\mathrm{eq}}$:

$$\exp\left(\frac{-A_i}{RT}\right) = \frac{\prod_j a_j^{\upsilon_{ij}}}{K_{i\,\mathrm{eq}}} \quad (4)$$

since the equilibrium coefficient is determined by the change in the standard state Gibbs free energies:

$$K_{i\,\mathrm{eq}} = \exp\left[\frac{-\sum_j \upsilon_{ij} G_j^o}{RT}\right] \quad (5)$$

For convenience, we define a dimensionless variable, z_i, equal to the exponential of $-A_i/RT$:

$$z_i = \exp\left(\frac{-A_i}{RT}\right) = \frac{\prod_j a_j^{\upsilon_{ij}}}{K_{i\,\mathrm{eq}}} \quad (6)$$

The value of z_i approaches zero as step i becomes irreversible, and as z_i approaches unity as step i becomes quasi-equilibrated; therefore, this value of z_i may be termed the reversibility of step i. We note that the definition of the reversibility, z_i, is simply a transform of the affinity, A_i, in the De Donder relation for step i. We also note that the value of z_i remains bounded between 0 and 1 provided that step i proceeds in the forward direction. If step i changes direction, then the value of z_i becomes >1. In such cases, it may be convenient to rewrite the step in the opposite direction so that the value of z_i remains <1.

This above approach can now be used to analyze the following reaction scheme for ethane hydrogenolysis over Pt:

1. $CH_3CH_3 + 2* \rightleftharpoons CH_2CH_3* + H*$
2. $CH_2CH_3* + 2* \rightleftharpoons CH_2CH_2*_2 + H*$
3. $CH_2CH_2*_2 + 2* \rightleftharpoons CHCH_2*_3 + H*$
4. $CHCH_2*_3 + 2* \rightleftharpoons CCH_2*_4 + H*$
5. $CH_2CH_2*_2 \rightleftharpoons CHCH_3*_2$
6. $CHCH_2*_3 \rightleftharpoons CCH_3*_3$
7. $CH_2CH_3* + 2* \rightarrow CH_2*_2 + CH_3*$
8. $CH_2CH_2*_2 + 2* \rightarrow CH_2*_2 + CH_2*_2$
9. $CHCH_3*_2 + 2* \rightarrow CH_3* + CH_3*$
10. $CHCH_2*_3 + 2* \rightarrow CH_3* + CH_2*_2$
11. $H_2 + 2* \rightleftharpoons 2H*$

where $*$ represents a vacant surface site. Steps 1–4 are dehydrogenation processes, steps 5 and 6 are isomerization processes, steps 7–9 are C–C bond cleavage steps, and step 11 is the adsorption of dihydrogen on the surface. Note that isomerization steps 5 and 6 may, in fact, involve hydrogenation-dehydrogenation steps, i.e. $CHCH_3*_2$ may be formed by dehydrogenation of $CH_2CH_2*_2$ to form $CHCH_2*_3$, followed by hydrogenation of $CHCH_2*_3$ to from $CHCH_3*_2$. The above reaction scheme involves four possible routes for ethane hydrogenolysis, since C–C bond cleavage may occur in four separate adsorbed species. Our previous work has shown that the activation barrier for a fifth possible route for C–C bond cleavage involving adsorbed CCH_2 species is considerably higher than the barriers for the other four routes, and hence, we do not include that route [16]. In this reaction scheme, we allow for the possibility that the most abundant adsorbed C_2H_x surface species is not necessarily the primary species that undergoes C–C bond cleavage. Finally, it is assumed for simplicity that mono-carbon species CH_x* are rapidly converted to methane, making steps 7–10 irreversible.

This 11-step reaction scheme involves seven reversible steps and four irreversible steps, giving rise to 18 rate coefficients, k_i. We note that each rate coefficient is composed of a pre-exponential factor and an activation energy, giving rise to two kinetic parameters for each rate coefficient. Next, we address the factors controlling the number of rate coefficients that must be known to conduct reaction kinetics analyses using this reaction scheme.

At steady state, the rates of formation are equal to the rates of consumption for each surface species.

The net rates of steps 4 and 6 are zero, since ethylidyne species, $CCH_3{*_3}$, and di-σ/π vinylidene species, $CCH_2{*_4}$, do not readily undergo C–C bond cleavage, i.e. these species are spectator species on the catalyst surface. Accordingly, z_4 and z_6 are equal to one.

Using De Donder relations, the following seven relations may be written for the fractional surface coverages by the various adsorbed species:

$$\theta_{\mathrm{H}} = \sqrt{K_{11\mathrm{eq}} z_{11} P_{\mathrm{H_2}}}\,\theta_* \tag{7}$$

$$\theta_{\mathrm{CH_2CH_3}} = K_{1\mathrm{eq}} z_1 \frac{P_{\mathrm{CH_3CH_3}}}{\sqrt{K_{11\mathrm{eq}} z_{11} P_{\mathrm{H_2}}}}\theta_* \tag{8}$$

$$\theta_{\mathrm{CH_2CH_2}} = K_{1\mathrm{eq}} K_{2\mathrm{eq}} z_1 z_2 \frac{P_{\mathrm{CH_3CH_3}}}{K_{11\mathrm{eq}} z_{11} P_{\mathrm{H_2}}}\theta_*^2 \tag{9}$$

$$\theta_{\mathrm{CHCH_3}} = K_{1\mathrm{eq}} K_{2\mathrm{eq}} K_{5\mathrm{eq}} z_1 z_2 z_5 \frac{P_{\mathrm{CH_3CH_3}}}{K_{11\mathrm{eq}} z_{11} P_{\mathrm{H_2}}}\theta_*^2 \tag{10}$$

$$\theta_{\mathrm{CHCH_2}} = K_{1\mathrm{eq}} K_{2\mathrm{eq}} K_{3\mathrm{eq}} z_1 z_2 z_3 \frac{P_{\mathrm{CH_3CH_3}}}{K_{11\mathrm{eq}}^{3/2} z_{11}^{3/2} P_{\mathrm{H_2}}^{3/2}}\theta_*^3 \tag{11}$$

$$\theta_{\mathrm{CCH_3}} = K_{1\mathrm{eq}} K_{2\mathrm{eq}} K_{3\mathrm{eq}} K_{6\mathrm{eq}} z_1 z_2 z_3 \times \frac{P_{\mathrm{CH_3CH_3}}}{K_{11\mathrm{eq}}^{3/2} z_{11}^{3/2} P_{\mathrm{H_2}}^{3/2}}\theta_*^3 \tag{12}$$

$$\theta_{\mathrm{CCH_2}} = K_{1\mathrm{eq}} K_{2\mathrm{eq}} K_{3\mathrm{eq}} K_{4\mathrm{eq}} z_1 z_2 z_3 \times \frac{P_{\mathrm{CH_3CH_3}}}{K_{11\mathrm{eq}}^{2} z_{11}^{2} P_{\mathrm{H_2}}^{2}}\theta_*^4 \tag{13}$$

Note that these relations for the surface coverages by C_2H_x species involve products of equilibrium coefficients, $K_{i\mathrm{eq}}$, that can be grouped into lumped equilibrium coefficients, $C_{i\mathrm{eq}}$:

$$\theta_{\mathrm{CH_2CH_3}} = C_{1\mathrm{eq}} z_1 \frac{P_{\mathrm{CH_3CH_3}}}{\sqrt{z_{11} P_{\mathrm{H_2}}}}\theta_* \tag{14}$$

$$\theta_{\mathrm{CH_2CH_2}} = C_{2\mathrm{eq}} z_1 z_2 \frac{P_{\mathrm{CH_3CH_3}}}{z_{11} P_{\mathrm{H_2}}}\theta_*^2 \tag{15}$$

$$\theta_{\mathrm{CHCH_3}} = C_{3\mathrm{eq}} z_1 z_2 z_5 \frac{P_{\mathrm{CH_3CH_3}}}{z_{11} P_{\mathrm{H_2}}}\theta_*^2 \tag{16}$$

$$\theta_{\mathrm{CHCH_2}} = C_{4\mathrm{eq}} z_1 z_2 z_3 \frac{P_{\mathrm{CH_3CH_3}}}{z_{11}^{3/2} P_{\mathrm{H_2}}^{3/2}}\theta_*^3 \tag{17}$$

$$\theta_{\mathrm{CCH_3}} = C_{5\mathrm{eq}} z_1 z_2 z_3 \frac{P_{\mathrm{CH_3CH_3}}}{z_{11}^{3/2} P_{\mathrm{H_2}}^{3/2}}\theta_*^3 \tag{18}$$

$$\theta_{\mathrm{CCH_2}} = C_{6\mathrm{eq}} z_1 z_2 z_3 \frac{P_{\mathrm{CH_3CH_3}}}{z_{11}^{2} P_{\mathrm{H_2}}^{2}}\theta_*^4 \tag{19}$$

$$\theta_{\mathrm{H}} = C_{7\mathrm{eq}} \sqrt{z_{11} P_{\mathrm{H_2}}}\,\theta_* \tag{20}$$

These coefficients $C_{i\mathrm{eq}}$ correspond to equilibrium coefficients for the following overall reactions:

Lumped reactions that control surface coverages, $\theta_{C_2H_x}$, and θ_{H}:

S1. $CH_3CH_3 + * \rightleftharpoons CH_2CH_3{*} + \frac{1}{2}H_2$
S2. $CH_3CH_3 + 2* \rightleftharpoons CH_2CH_2{*_2} + H_2$
S3. $CH_3CH_3 + 2* \rightleftharpoons CHCH_3{*_2} + H_2$
S4. $CH_3CH_3 + 3* \rightleftharpoons CHCH_2{*_3} + \frac{3}{2}H_2$
S5. $CH_3CH_3 + 3* \rightleftharpoons CCH_3{*_3} + \frac{3}{2}H_2$
S6. $CH_3CH_3 + 4* \rightleftharpoons CCH_2{*_4} + 2H_2$
S7. $H_2 + 2* \rightleftharpoons 2H*$

The non-zero net rates of the elementary steps are given by

$$r_1 = k_1 P_{\mathrm{CH_3CH_3}} \theta_*^2 (1 - z_1) \tag{21}$$

$$r_2 = k_2 K_{1\mathrm{eq}} z_1 \frac{P_{\mathrm{CH_3CH_3}}}{\sqrt{K_{11\mathrm{eq}} z_{11} P_{\mathrm{H_2}}}}\theta_*^3 (1 - z_2) \tag{22}$$

$$r_3 = k_3 K_{1\mathrm{eq}} K_{2\mathrm{eq}} z_1 z_2 \frac{P_{\mathrm{CH_3CH_3}}}{K_{11\mathrm{eq}} z_{11} P_{\mathrm{H_2}}}\theta_*^4 (1 - z_3) \tag{23}$$

$$r_5 = k_5 K_{1\mathrm{eq}} K_{2\mathrm{eq}} z_1 z_2 \frac{P_{\mathrm{CH_3CH_3}}}{K_{11\mathrm{eq}} z_{11} P_{\mathrm{H_2}}}\theta_*^2 (1 - z_5) \tag{24}$$

$$r_7 = k_7 K_{1\mathrm{eq}} z_1 \frac{P_{\mathrm{CH_3CH_3}}}{\sqrt{K_{11\mathrm{eq}} z_{11} P_{\mathrm{H_2}}}}\theta_*^3 \tag{25}$$

$$r_8 = k_8 K_{1\mathrm{eq}} K_{2\mathrm{eq}} z_1 z_2 \frac{P_{\mathrm{CH_3CH_3}}}{K_{11\mathrm{eq}} z_{11} P_{\mathrm{H_2}}}\theta_*^4 \tag{26}$$

$$r_9 = k_9 K_{1\mathrm{eq}} K_{2\mathrm{eq}} K_{5\mathrm{eq}} z_1 z_2 z_4 \frac{P_{\mathrm{CH_3CH_3}}}{K_{11\mathrm{eq}} z_{11} P_{\mathrm{H_2}}}\theta_*^4 \tag{27}$$

$$r_{10} = k_{10} K_{1\mathrm{eq}} K_{2\mathrm{eq}} K_{3\mathrm{eq}} z_1 z_2 z_3 \frac{P_{\mathrm{CH_3CH_3}}}{K_{11\mathrm{eq}}^{3/2} z_{11}^{3/2} P_{\mathrm{H_2}}^{3/2}}\theta_*^5 \tag{28}$$

$$r_{11} = k_{11} K_{11\mathrm{eq}} z_{11} P_{\mathrm{H_2}} \theta_*^2 (1 - z_{11}) \tag{29}$$

Once again, it is recognized that a product of rate and equilibrium coefficients can be replaced by a single,

lumped coefficient; therefore, the non-zero net rates of steps 1–11 are written in terms of nine lumped coefficients, C_i:

$$r_1 = C_1 P_{CH_3CH_3} \theta_*^2 (1 - z_1) \quad (30)$$

$$r_2 = C_2 z_1 \frac{P_{CH_3CH_3}}{\sqrt{z_{11} P_{H_2}}} \theta_*^3 (1 - z_2) \quad (31)$$

$$r_3 = C_3 z_1 z_2 \frac{P_{CH_3CH_3}}{z_{11} P_{H_2}} \theta_*^4 (1 - z_3) \quad (32)$$

$$r_5 = C_4 z_1 z_2 \frac{P_{CH_3CH_3}}{z_{11} P_{H_2}} \theta_*^2 (1 - z_5) \quad (33)$$

$$r_7 = C_5 z_1 \frac{P_{CH_3CH_3}}{\sqrt{z_{11} P_{H_2}}} \theta_*^3 \quad (34)$$

$$r_8 = C_6 z_1 z_2 \frac{P_{CH_3CH_3}}{z_{11} P_{H_2}} \theta_*^4 \quad (35)$$

$$r_9 = C_7 z_1 z_2 z_5 \frac{P_{CH_3CH_3}}{z_{11} P_{H_2}} \theta_*^4 \quad (36)$$

$$r_{10} = C_8 z_1 z_2 z_3 \frac{P_{CH_3CH_3}}{z_{11}^{3/2} P_{H_2}^{3/2}} \theta_*^5 \quad (37)$$

$$r_{11} = C_9 z_{11} P_{H_2} \theta_*^2 (1 - z_{11}) \quad (38)$$

Finally, a site balance may be written to express θ_* in terms of fractional surface coverages by C_2H_x species (assuming that surface coverages by mono-carbon species CH_x species are negligible):

$$1 = \theta_* + \theta_H + \theta_{CH_2CH_3} + 2\theta_{CH_2CH_2} + 2\theta_{CHCH_3} + 3\theta_{CHCH_2} + 3\theta_{CCH_3} + 4\theta_{CCH_2} \quad (39)$$

At steady state, the rates of formation are equal to the rates of consumptions for each surface species, leading to the following relations:

$$\frac{d\theta_{CH_2CH_3}}{dt} = r_1 - r_2 - r_7 = 0 \quad (40)$$

$$\frac{d\theta_{CH_2CH_2}}{dt} = r_2 - r_3 - r_5 - r_8 = 0 \quad (41)$$

$$\frac{d\theta_{CHCH_2}}{dt} = r_3 - r_6 - r_{10} = 0 \quad (42)$$

$$\frac{d\theta_{CHCH_3}}{dt} = r_5 - r_9 = 0 \quad (43)$$

$$\frac{d\theta_H}{dt} = r_1 + r_2 + r_3 + r_4 - 3r_7 - 4r_8 - 4r_9 - 5r_{10} + 2r_{11} = 0 \quad (44)$$

To solve the kinetic model, we now have six equations (e.g. five steady state relations involving non-zero rates (Eqs. (40)–(44)) and one site balance (Eq. (39)) and six unknowns (z_1, z_2, z_3, z_5, z_{11} and θ_*).

It can now be seen that the maximum number of kinetic coefficients required for the analysis is equal to nine (corresponding to C_1 through C_9), plus one additional coefficient ($C_{i\,eq}$) for each species that is non-negligible in the site balance. For example, the maximum number of kinetic coefficients is equal to 11, if H^* and $CCH_3{*_3}$ are the most abundant surface species.

The number of kinetic coefficients required for kinetic analyses decreases further if various steps become quasi-equilibrated. For example, if we assume that H^* and $CCH_3{*_3}$ remain the most abundant surface species, then the number of significant kinetic coefficients decreases from 11 to 7 if the hydrogenation–dehydrogenation steps and the dihydrogen desorption step are assumed to be quasi-equilibrated. The number of significant kinetic coefficients decreases from seven to six if the isomerization step 5 is also assumed to be quasi-equilibrated. Finally, the number of kinetically significant coefficients decreases from six to three if only one of the C–C bond cleavage routes (e.g. cleavage of $CHCH_3{*_2}$ species) is important.

According to transition state theory, we may express the forward rate coefficient for a given step in terms of an equilibrium relation between the reactants and the activated complex for that step. Therefore, kinetic coefficients C_5 through C_8 can be expressed in terms of quasi-equilibrium coefficients, $K_{C_2H_x^\ddagger}$:

$$C_5 = \frac{k_7 K_{1eq}}{\sqrt{K_{11eq}}} = \nu^\ddagger K_{CH_2CH_5^\ddagger} \quad (45)$$

$$C_6 = \frac{k_8 K_{1eq} K_{2eq}}{K_{11eq}} = \nu^\ddagger K_{CH_2CH_2^\ddagger} \quad (46)$$

$$C_7 = \frac{k_9 K_{1eq} K_{2eq} K_{5eq}}{K_{11eq}} = \nu^\ddagger K_{CHCH_3^\ddagger} \quad (47)$$

$$C_8 = \frac{k_{10} K_{1eq} K_{2eq} K_{3eq}}{K_{11eq}^{3/2}} = \nu^\ddagger K_{CHCH_3^\ddagger} \quad (48)$$

where $\nu^{\ddagger}$ is a frequency factor, equal to $k_B T/h$, where k_B is Boltzmann constant, T is temperature, and h is Planck's constant. The four coefficients $K_{C_2H_x^{\ddagger}}$ refer to quasi-equilibrium coefficients for the following overall reactions:

Lumped quasi-equilibria that control the rate of C–C bond cleavage

T1. $CH_3CH_3 + 3* \rightleftharpoons CH_2CH_3^{\ddagger} *_3 \frac{1}{2}H_2$

T2. $CH_3CH_3 + 4* \rightleftharpoons CH_2CH_2^{\ddagger} *_4 H_2$

T3. $CH_3CH_3 + 4* \rightleftharpoons CHCH_3^{\ddagger} *_4 + H_2$

T4. $CH_3CH_3 + 5* \rightleftharpoons CHCH_2^{\ddagger} *_5 + \frac{3}{2}H_2$

Temperature effects may be taken into account for the lumped kinetic coefficients (C_i and $C_{i\,eq}$) by writing these coefficients in terms of the standard entropy and enthalpy changes for the formation of stable species and activated complexes:

$$C_i = \exp\left(\frac{\Delta S_i^o}{R}\right) \exp\left(\frac{-\Delta H_i}{RT}\right) \tag{49}$$

For example, the standard entropy changes for the formation of stable species (S1–S7) and activated complexes (T1–T4) can be expressed in terms of standard entropies of gaseous ethane and dihydrogen and standard entropies of the appropriate surface species and activated complexes. Similarly, the enthalpy changes for these steps may be written in terms of known gaseous enthalpies of ethane and dihydrogen and enthalpies of the appropriate surface species. An important advantage of using lumped kinetic coefficients (C_i and $C_{i\,eq}$) to conduct analyses of reaction schemes is that these coefficients minimize complications from unintentional compensation effects. For example, we consider the situation where step 11 (adsorption of H_2) is quasi-equilibrated, and the equilibrium surface coverage by atomic hydrogen is low (low pressures of H_2 and/or high temperatures). In this case, the lumped quasi-equilibria identified by De Donder analyses show that rate of ethane hydrogenolysis is independent of the properties of adsorbed H atoms. If the kinetic model had been formulated in terms of the individual rate coefficients for the elementary steps, then it would appear that the rates of specific steps might depend on the strength of interaction of atomic hydrogen with the surface, e.g. the reverse rate coefficients for steps 1–4 would be expected to decrease as the strength of interaction of hydrogen atoms with the surface increases. However, this decrease in reverse rate coefficients would be compensated by changes in the surfaces coverages by H$*$ and C_2H_x* species, such that the net rates of steps 1–4 are independent of the properties of adsorbed atomic hydrogen. Accordingly, the use of the proper lumped kinetic coefficients provides a more direct approach for identifying the factors controlling the kinetics of the catalytic process.

Another unintentional compensation effect would be introduced into the kinetic model by expressing the activation barrier for cleavage of the C–C bond in terms of the energy of the corresponding stable, adsorbed C_2H_x species. If this stable adsorbed C_2H_x species remains in low concentration on the surface, then we recognize from De Donder relations that the kinetic parameters controlling the surface coverage by this species are not significant. However, these kinetic parameters can appear to be significant if we relate the properties of the transition states to the properties of this stable, adsorbed species.

2.2. Application of theoretical results

Computational methods using density functional theory (DFT) have rapidly progressed owing to advances in computational speed, along with the development of new algorithms. For example, DFT methods have proven to be useful to predict accurate geometries and reasonable energetics for molecules containing transition metals [1,2,16,21–24]. The results of quantum chemical calculations, therefore, complement the results of experimental investigations of stable adsorbed species. Furthermore, these calculations can be used to predict the energetics of highly reactive intermediates and transition states that cannot be observed experimentally. Recent DFT computational studies have address the factors controlling the rate of ethane hydrogenolysis over Pt catalysts [16,25]. These DFT studies involved calculations to investigate the interactions of C_2H_x species with Pt_{10} clusters and Pt(1 1 1) and Pt(2 1 1) slabs.

Detailed descriptions about these DFT calculations can be found elsewhere [16]. Density functional theory calculations for Pt clusters were carried out with Jaguar software (Schrodinger, Inc.) [26]. The chosen density functional uses a hybrid method employing

Becke's three-parameter approach, B3LYP. The basis set employed in all calculations uses an effective core potential on all Pt atoms. The C and H atoms have been treated with the 6–31G** basis set, with all electrons being considered explicitly. Slab calculations [27] were conducted for both Pt(1 1 1) and Pt(2 1 1) surfaces. Calculations were performed on both two and three layer slabs, which were periodically repeated in a super cell geometry with four equivalent layers of vacuum between any two successive metal slabs. A 2×2 unit cell was used to study the adsorption of various species, corresponding to 1/4 monolayer coverage. Ionic cores are described by ultra-soft pseudopotentials, and the Kohn–Sham one-electron valence states are expanded in a basis of plane waves with kinetic energies below 25 Ry. The surface Brillouin zone is sampled at 18 special *k*-points. The exchange-correlation energy and potential are described by the generalized gradient approximation (PW-91).

These DFT calculations were used to determine the binding energies of experimentally observed surface species, such as di-σ bonded ethylene, ethylidyne species, and di-σ/π vinylidene species as well as the binding energies of the other unobserved species, such as ethyl, ethylidene and vinyl species, that are postulated to be reactive intermediates in surface [16,25]. Furthermore, these calculations predicted activation energies for C–C bond dissociation of various adsorbed C_2H_x species. Importantly, it was shown that the bonding energies are dependent on the geometry of the surface, leading to the observed structure sensitivity of ethane hydrogenolysis [16].

The results from our DFT calculations for various stable C_2H_x species and transitions states on Pt(1 1 1) and Pt(2 1 1) surfaces are summarized in Table 1. This table also shows entropy changes for the various steps, as estimated from DFT calculations of the vibrational frequencies for the various C_2H_x species and transition states on 10-atom Pt clusters [16]. In addition, Table 1 shows estimates of the standard Gibbs free energy changes for the formation of stable C_2H_x surface species and activated complexes responsible for C–C bond cleavage at 623 K. These estimates were made by combining the energetic information obtained from DFT calculations involving C_2H_x species on Pt slabs, with entropic information obtained from DFT calculations involving C_2H_x species on Pt clusters. In can be seen in Table 1 that the processes with the most favorable changes in Gibbs free energies are steps S7 and S5, i.e. the formation of atomic hydrogen and ethylidyne species ($^*CCH_3$) on Pt. In contrast, the lowest Gibbs free energy barrier for cleavage of the C–C bond is through the activated complex based on ethyl species ($^*C_2H_5^{\ddagger}$). Additionally, Table 1 shows that the calculated values of the activation barriers are significantly lower on Pt(2 1 1) compared to

Table 1
Summary of DFT calculation results [16] for reactions of ethane over Pt(1 1 1) and Pt(2 1 1) surfaces[a]

Reaction	$\Delta E_{electronic}$ (kJ/mol)		ΔH (kJ/mol)		ΔS^o (J/mol/K)	ΔG^o (kJ/mol)	
	(1 1 1)	(2 1 1)	(1 1 1)	(2 1 1)		(1 1 1)	(2 1 1)
S1. $C_2H_6+*\langle\rangle \rightarrow {}^*C_2H_5+0.5H_2$	51	6	46	1	−92	103	58
S2. $C_2H_6+*\langle\rangle \rightarrow {}^*C_2H_4+H_2$	70	−1	53	−18	−43	80	9
S3. $C_2H_6+*\langle\rangle \rightarrow {}^*CHCH_3+H_2$	104	19	77	−8	−33	98	13
S4. $C_2H_6+*\langle\rangle \rightarrow {}^*CHCH_2+1.5H_2$	128	80	97	49	18	86	38
S5. $C_2H_6+*\langle\rangle \rightarrow {}^*CCH_3+1.5H_2$	58	45	30	17	35	8	−5
S6. $C_2H_6+*\langle\rangle \rightarrow {}^*CCH_2+2H_2$	157	138	119	100	86	65	46
S7. $H_2+2*\langle\rangle \rightarrow +2H*$	−85	−146	−91		−119	−17	
T1. $C_2H_6+*\langle\rangle \rightarrow {}^*C_2H_5^{\ddagger}+0.5H_2$	224	108	213	97	−107	280	164
T2. $C_2H_6+*\langle\rangle \rightarrow {}^*C_2H_4^{\ddagger}+H_2$		192		168	−40		193
T3. $C_2H_6+*\langle\rangle \rightarrow {}^*CHCH_3^{\ddagger}+H_2$	210	182	187	159	−43	214	186
T4. $C_2H_6+*\langle\rangle \rightarrow {}^*CHCH_2^{\ddagger}+1.5H_2$	288	241	253	206	16	242	196

[a] Thermodynamic properties (ΔH, ΔS^o, and ΔG^o) determined at 623 K and 1 atm. The calculated standard entropies (1 atm, 623 K) for gaseous ethane and dihydrogen are 278 and 152 J/mol/K, respectively.

Pt(1 1 1), illustrating the structure sensitivity of ethane hydrogenolysis over platinum-based materials.

The results of our DFT calculations predict that the primary pathways for C–C bond cleavage involve activated complexes that are more highly hydrogenated (e.g. adsorbed $CHCH_3$ and C_2H_5 species) compared to the most abundant surface intermediates (e.g. adsorbed CCH_3). Accordingly, the adsorbed C_2H_x reactive species that are responsible for C–C bond cleavage are not necessarily the most abundant surface intermediates that can be observed spectroscopically. However, the most abundant surface intermediates (e.g. adsorbed atomic hydrogen and CCH_3) still play an important role in the reaction kinetics by determining the fraction of the surface that is available for catalytic reaction (i.e. they participate in site blocking).

2.3. Reaction scheme for ethane hydrogenolysis

Based on the results from our DFT calculations, we have employed the reaction scheme shown in Table 2 to describe our reaction kinetic data for ethane hydrogenolysis over Pt. This reaction scheme incorporates the quasi-equilibrated formation of C_2H_x species with $2 \leq x \leq 5$ and C–C bond cleavage of C_2H_x species with $3 \leq x \leq 5$. As shown above, the surface coverages by stable C_2H_x species and activated complexes for C–C cleavage of C_2H_x species are expressed in terms of quasi-equilibrium coefficients and the partial pressures of ethane and dihydrogen.

2.4. Parameterization of the kinetic model

In view of the present accuracy of quantum chemical calculations, it is typically necessary to adjust the initial estimates of the potential energy surface to describe the observed kinetics of a catalytic process. Accordingly, the theoretical results presented in Table 1 provide initial guesses for the entropies and enthalpies of the stable species and reactive intermediates involved in ethane hydrogenolysis over platinum. In the present kinetic analysis, the entropies of surface species were adjusted by two fitting parameters: (1) a multiplicative factor applied to the DFT-predicted entropies for stable C_2H_x species; and (2) a multiplicative factor applied to the DFT-predicted entropies of activated complexes. Additionally, the enthalpy changes for the eight quasi-equilibrated steps shown in Table 2 were varied. For the stable adsorbed species, we have used the energetic properties corresponding to the most favorable Gibbs free energy for a given stoichiometry. For example, we have included the coverage of di-σ bonded ethylene species, $^*C_2H_4$, instead of the vinylidene species, $^*CHCH_3$. However, the transition state for cleavage of the C–C bond in adsorbed $^*C_2H_4$ species has a higher Gibbs free

Table 2
Fitted parameters for ethane hydrogenolysis over Pt/SiO_2 at 623 K

Reaction	ΔS^o (J/mol/K)	ΔH (kJ/mol)	ΔG^o (kJ/mol)	ΔG^o Difference[f] (kJ/mol)
S1. $C_2H_6+*\langle\!\rangle$ $^*C_2H_5+0.5H_2$	−47[b]	1[d]	30	28
S2. $C_2H_6+*\langle\!\rangle$ $^*C_2H_4+H_2$	−9[b]	−4 ± 6	2	7
S5. $C_2H_6+*\langle\!\rangle$ $^*CCH_3+1.5H_2$	69[b]	−44 ± 11	1	−6
S6. $C_2H_6+*\langle\!\rangle$ $^*CCH_2+2H_2$	110[b]	100[d]	31	15
S7. $H_2+2*\langle\!\rangle$ $+2H*$	−68[a] (constrained)	−54 ± 6.4	−12	−5
T1. $C_2H_6+*\langle\!\rangle$ $^*C_2H_5^{\ddagger}+0.5H_2$	−120[c]	82 ± 14	159	5
T3. $C_2H_6+*\langle\!\rangle$ $^*CHCH_3^{\ddagger}+H_2$	−55[c]	109[e] (constrained)	143	43
T4. $C_2H_6+*\langle\!\rangle$ $^*CHCH_2^{\ddagger}+1.5H_2$	7[c]	156[e] (constrained)	151	44

[a] Value constrained such that adsorbed hydrogen does not exceed 2° of translational mobility.

[b] Fitted parameter is ratio of surface entropy to the DFT-predicted entropy for the adsorbed species. The value of this parameter was found to be 1.41 ± 0.15.

[c] Fitted parameter is ratio of surface entropy of the activated complex to the DFT-predicted entropy for that activated complex. The value of this parameter was found to be 0.86 ± 0.13.

[d] Parameters maintained at values predicted by DFT calculations (see Table 1).

[e] Value constrained to be within 50 kJ/mol of theoretical value.

[f] Difference between theoretical ΔG^o (see Table 1) and the fitted ΔG^o of this table.

energy than the transition state for adsorbed $^*CHCH_3$ species. Therefore, we have expressed C–C bond cleavage through the activated vinylidene species rather than the activated di-σ bonded ethylene.

2.5. Results of the kinetic analysis

Values for the fitted parameters were determined using Athena Visual Workbench [28]. This software employs a general regression analysis of the reaction kinetics data with the reactor treated as a continuous stirred-tank reactor. All values of the parameters were estimated at the average reactor temperature of 623 K.

Figs. 1 and 2 show comparisons of the predicted (depicted by the solid lines) versus experimentally observed rates of ethane hydrogenolysis over Pt/SiO_2. These figures show the change of the methane production rate with respect to the ethane and hydrogen pressures at 573, 623, and 673 K. Tests were conducted at replicate conditions to track possible changes in catalyst reactivity (e.g. deactivation). Data points for these replicate tests are shown in Figs. 1 and 2. The experimental error determined from these points was <6%. Fig. 1 shows negative hydrogen pressure dependencies at higher hydrogen pressures and lower temperatures. Furthermore, this figure shows that the hydrogen orders become less negative at lower hydrogen pressures and higher temperatures. Fig. 2 shows that the ethane pressure dependence decreases from ca. 1.0 to 0.0 as the temperature increases from 573 to 673 K for

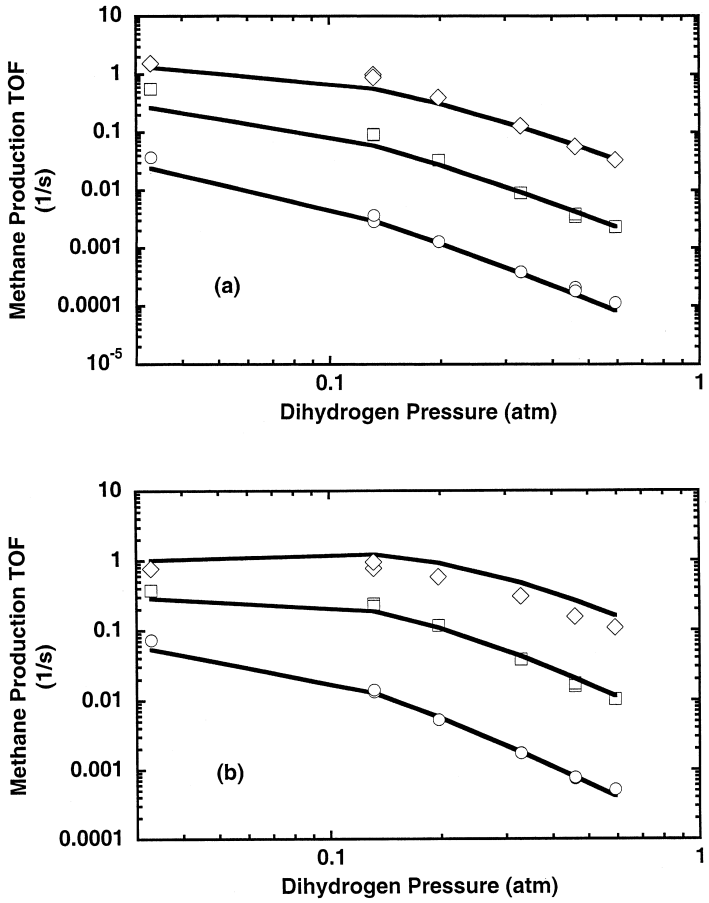

Fig. 1. Dihydrogen pressure dependencies for ethane hydrogenolysis at (a) 0.0066 atm and (b) 0.033 atm ethane pressures (experimental results: (○) 573 K; (□) 623 K; and (◇) 673 K). Predicted rates given by solid line.

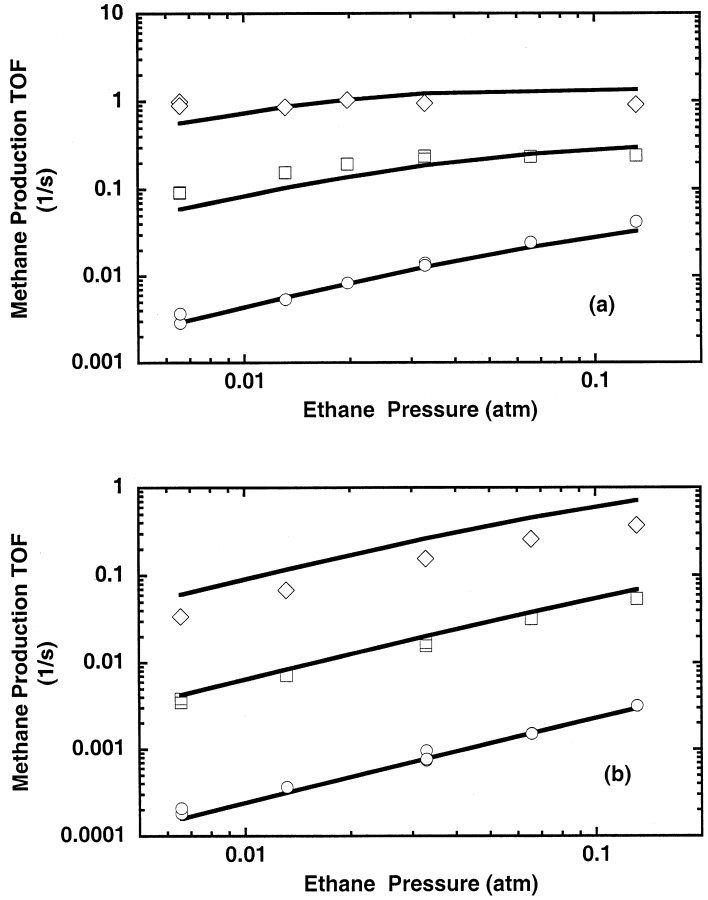

Fig. 2. Ethane pressure dependencies for ethane hydrogenolysis at (a) 0.13 atm and (b) 0.46 atm dihydrogen pressure (experimental results: (○) 573 K; (□) 623 K; and (◇) 673 K). Predicted rates given by solid line.

a hydrogen pressure of 0.13 atm. In contrast, this figure shows that the ethane kinetic orders are near unity at all temperatures at the higher hydrogen pressure of 0.46 atm.

Table 2 lists the values of the fixed and fitted parameters, along with 95% confidence limits for the fitted parameters. The surface coverages of the stable C_2H_5 and CCH_2 adsorbed species are predicted to be low; therefore, the overall rate was not sensitive to the enthalpy changes to form these surface species, and the values for these enthalpy changes were maintained at the theoretically predicted values. In this simulation, the surface entropy for adsorbed hydrogen was constrained to not exceed a value corresponding to two degrees of translational freedom (mobile adsorption). The resulting enthalpy change for hydrogen adsorption was fitted to a value of −54 kJ/mol. The kinetic analyses predict that the surface should be largely covered with atomic hydrogen (fractional coverage of 0.55). Results from previous microcalorimetric studies of hydrogen adsorption on silica-supported platinum indicate that the fitted standard entropy and enthalpy changes are reasonable at this average coverage [29–32]. Furthermore, Table 2 shows comparisons between the theoretically predicted and the fitted free energy changes. For the adsorption of hydrogen, this free energy comparison shows good agreement between the predicted value and fitted value. Similarly, Table 2 shows good agreement between theory and the fitted values for the free energy changes involved

in the formation of stable CCH_3 and C_2H_4 species on the surface. The results in Table 2 indicate that the mobilities for the stable adsorbed C_2H_x species are higher than the predicted values, since the value of the multiplicative factor applied to the standard surface entropies of these stable species was found to be 1.41. This multiplicative factor results in fitted values for the surface entropies of the stable species that correspond to species with one degree of translational freedom on the surface. Table 2 also indicates that the fit of the kinetic data utilizes slightly lower entropies for the transition states compared to theoretical predictions, since the multiplicative factor applied to the standard surface entropies of these transition states was found to be 0.86. These results indicate that the transition states are essentially immobile species.

The largest differences between the theoretical predictions and the results of the kinetic analysis are in the enthalpy changes to form the transition states from gas-phase ethane. The theoretically predicted enthalpy changes for the formation of C_2H_x transition states were too large to achieve the measured rate of ethane hydrogenolysis. Accordingly, these enthalpy changes were allowed to decrease, but they were constrained to remain within 50 kJ/mol of the theoretical values. The results of the DFT calculations predict that the preferred reaction pathway for cleavage of the C–C bond involves adsorbed C_2H_5 species, while the results from kinetic analyses suggest that the preferred reaction pathway involves adsorbed $CHCH_3$ species. Importantly, the results from DFT calculations and the kinetic analyses agree that C–C bond cleavage takes place through C_2H_x species that are more hydrogenated than the most abundant C_2H_x species on the surface.

3. Discussion

The results from De Donder analyses of a general reaction scheme for ethane hydrogenolysis indicate that the rate of the overall reaction can be described in terms of a series of lumped reaction steps involving the formation of stable C_2H_x adsorbed species and transition states from gas-phase ethane and dihydrogen. Over Pt catalysts, these lumped reactions to form stable C_2H_x adsorbed species are quasi-equilibrated, since deuterium tracing experiments show that exchange reactions between ethane and deuterium to yield deuterated ethane occur at higher rates than the rate of the hydrogenolysis reaction. In particular, Zaera and Somorjai [33] showed that the deuterium exchange rates were three orders of magnitude faster than the rate of ethane hydrogenolysis over Pt(1 1 1) at temperatures between 475 and 625 K.

The formation of surface intermediates in quasi-equilibrium with gas-phase ethane and dihydrogen was proposed by Cimino et al. [15]. As mentioned above, this mechanism involves the quasi-equilibrated formation of a most abundant reactive intermediate that undergoes C–C bond cleavage. Sinfelt [7,8] used a variation of this mechanism to analyze kinetic data for ethane hydrogenolysis over a variety of metal catalysts, and estimated values of x for the adsorbed C_2H_x reactive intermediates on these metals. Results from kinetic analyses by Sinfelt over Pt suggested that the rate-limiting step involved a highly dehydrogenated C_2H_x intermediate [7]. The results of DFT calculations presented in Table 1 suggest that the most abundant stable C_2H_x surface species are not necessarily the most reactive species. In particular, the most abundant species on the surface are predicted to be atomic hydrogen and CCH_3 species, whereas C–C bond cleavage is predicted to take place through C_2H_5 species, with contributions also from $CHCH_3$ and/or C_2H_3 species. While the most abundant surface species (e.g. adsorbed atomic hydrogen and ethylidyne species) are not directly involved in the primary reaction pathways, they affect the observed kinetic rates through blocking of sites.

More recent results of NMR investigations conducted by Klug et al. [34] in conjunction with Sinfelt suggest that the C–C bond breaking step may involve an adsorbed C_2H_x species with $x = 3$ over platinum. In this more recent investigation, it was demonstrated that ethylidyne (CCH_3) species form upon adsorption of acetylene on platinum, and it was suggested that these ethylidyne species may play a role in the C–C bond scission of acetylene [34]. Our kinetic model for ethane hydrogenolysis over Pt, based on lumped reactions identified by De Donder analysis and utilizing initial guesses for kinetic parameters from results of DFT calculations, provides a good description of the reaction kinetics data collected over a wide range of reaction conditions. The primary difference between the values of the final kinetic parameters used in the

model and the initial values obtained from DFT calculations was that the fitted enthalpy changes for the formation of C_2H_x transition states involved in cleavage of the C–C bond were lower than the initial values predicted from DFT calculations. This difference may be caused by the observed structure sensitivity of the ethane hydrogenolysis over metals. In fact, Table 1 shows significant differences between the binding energies on Pt(1 1 1) and Pt(2 1 1) for various adsorbates and transition states. In general, the hydrocarbon species and transition states are held more strongly on the step edge of the Pt(2 1 1) surface compared to the Pt(1 1 1) surface, leading to higher reactivity of defect sites like the step edge of Pt(2 1 1). Accordingly, the studied Pt catalyst may contain Pt surface atoms with even higher reactivity than the sites present on the Pt(2 1 1) surface. It must also be noted that the errors involved in the DFT calculations may contribute to the differences in the predicted and experimental values. For example, the calculated bonding energetics are dependent on the functional used to describe the effects of electron exchange and correlation.

Finally, the kinetic analyses presented in this study were based on the assumption of a uniform surface that follows Langmuiran kinetics. This simplification may not be completely justified, since the kinetic analyses suggest that the surface is highly covered with adsorbed hydrogen atoms and/or hydrocarbon species. Furthermore, this analysis involves intermediates and transition states that interact with three, four, or five Pt atoms to explain the observed variations in the overall rate with respect to the dihydrogen and ethane pressures. Accordingly, the next step for the analysis of this system may be to use the results from DFT calculations in conjunction with Monte Carlo calculations to predict the observed reaction kinetics data.

4. Conclusions

The principles of De Donder can be applied to a general reaction scheme of elementary steps for ethane hydrogenolysis over Pt to identify a set of kinetic coefficients that explain the observed reaction kinetics. These kinetic coefficients are expressed in terms of lumped reaction steps involving the formation of stable adsorbed species and transition states from gaseous ethane and dihydrogen. Values for the standard entropy and enthalpy changes for these steps are predicted from DFT calculations of the interactions of the appropriate species with Pt(1 1 1) and Pt(2 1 1) slabs. The results of these DFT calculations suggest that the primary pathways for C–C bond cleavage may take place through activated complexes that are more highly hydrogenated (e.g. C_2H_5 and $CHCH_3$) compared to the most abundant surface intermediates (e.g. CCH_3). Accordingly, the reactive species that are responsible for C–C bond cleavage are not necessarily the most abundant surface intermediates that can be observed spectroscopically. However, these most abundant surface intermediates still play an important role in the reaction kinetics by determining the fraction of the surface that is available for catalytic reaction (i.e. they participate in site blocking). The initial values for most of the kinetic parameters obtained from DFT calculations provide a good description for the reaction kinetics data collected over a wide range of reaction conditions. The primary difference between the values of the final kinetic parameters used in the model and the initial values obtained from DFT calculations was that the fitted enthalpy changes for the formation of C_2H_x transition states involved in cleavage of the C–C bond were lower than the initial values predicted from DFT calculations. This difference may be explained by the structure sensitivity of the system and/or the inherent error of the DFT calculations. The analyses of this study provide a description at the molecular-level of the catalytic chemistry involved in ethane hydrogenolysis over Pt, and this description may be useful for further studies of hydrocarbon reactions on metal surfaces.

Acknowledgements

We acknowledge financial support for the experimental work of this research by the National Science Foundation and financial support for the modeling work of this research by the National Center for Clean Industrial and Treatment Technologies. We thank Professor Jens Norskov for help with DFT slab calculations.

References

[1] M. Neurock, R.A. van Santen, Catal. Today 50 (1999) 445.

[2] J.K. Norskov, Stud. Surf. Sci. Catal. 122 (1999) 3.
[3] G.A. Somorjai, Introduction to Surface Chemistry and Catalysis, Wiley, New York, 1994.
[4] R.I. Masel, Principles of Adsorption and Reaction on Solid Surfaces, Wiley, New York, 1996.
[5] J.H. Sinfelt, W.F. Taylor, D.J.C. Yates, J. Phys. Chem. 69 (1) (1965) 95.
[6] J.H. Sinfelt, D.J.C. Yates, J. Catal. 8 (1967) 82.
[7] J.H. Sinfelt, J. Catal. 27 (1972) 468.
[8] J.H. Sinfelt, Adv. Catal. 23 (1973) 91.
[9] S.A. Goddard, M.D. Amiridis, J.E. Rekoske, N. Cardona-Martinez, J.A. Dumesic, J. Catal. 117 (1989) 155.
[10] G.C. Bond, M.R. Gelsthorpe, Faraday Trans. I 85 (11) (1989) 3767.
[11] G.C. Bond, R.H. Cunningham, J. Catal. 163 (1996) 328.
[12] G.C. Bond, A.D. Hooper, J.C. Slaa, A.O. Taylor, J. Catal. 163 (1996) 319.
[13] S.B. Shang, C.N. Kenney, J. Catal. 134 (1992) 134.
[14] R.D. Cortright, R.M. Watwe, B.E. Spiewak, J.A. Dumesic, Catal. Today 53 (1999) 395.
[15] A. Cimino, M. Boudart, H.S. Taylor, J. Phys. Chem. 58 (1954) 796.
[16] R.M. Watwe, R.D. Cortright, J.K. Nørskov, J.A. Dumesic, J. Phys. Chem. B 104 (2000) 2299.
[17] T. De Donder, L'Affinite, Gauthier-Villers, Paris, 1927, p. 43.
[18] M. Boudart, J. Phys. Chem. 87 (1983) 2786.
[19] W.L. Holstein, M. Boudart, J. Phys. Chem. B 101 (1997) 9991.
[20] J.A. Dumesic, J. Catal. 185 (2) (1999) 496.
[21] R.M. Watwe, H.S. Bengaard, J.R. Rostrup-Nielsen, J.A. Dumesic, J.K. Norskov, J. Catal. 189 (2000) 16.
[22] R.A. van Santen, M. Neurock, Catal. Rev. Sci. Eng. 37 (4) (1995) 557.
[23] J.F. Paul, P. Sautet, J. Phys. Chem. B 102 (1998) 1578.
[24] P.E.M. Siegbahn, Adv. Chem. Phys. XCIII (1996) 333.
[25] R.M. Watwe, B.E. Spiewak, R.D. Cortright, J.A. Dumesic, J. Catal. 180 (1998) 184.
[26] Jaguar 3.5, Schrodinger, Portland, OR, 1998.
[27] B. Hammer, L.B. Hansen, J.K. Nørskov, Phys. Rev. B 59 (1999) 7413.
[28] M.C. Caracotsios, W.A. Stewart, Athena Visual Workbench 2.0, Stewart and Associates, Madison, WI, 1999.
[29] S.B. Sharma, J.T. Miller, J.A. Dumesic, J. Catal. 148 (1994) 198.
[30] R.D. Cortright, J.A. Dumesic, J. Catal. 148 (1994) 771.
[31] M.A. Natal-Santiago, S.G. Podkolzin, R.D. Cortright, J.A. Dumesic, Catal. Lett. 45 (1997) 155.
[32] B.E. Spiewak, R.D. Cortright, J.A. Dumesic, J. Catal. 176 (1998) 405.
[33] F. Zaera, G.A. Somorjai, J. Phys. Chem. 89 (1985) 3211.
[34] C.A. Klug, C.P. Slichter, J.H. Sinfelt, J. Phys. Chem. 95 (1991) 2119.